

Full length article

Site classification for National Strong Motion Observation Network System (NSMONS) stations in China using an empirical H/V spectral ratio method

Kun Ji¹, Yefei Ren^{*}, Ruizhi Wen²

Institute of Engineering Mechanics, China Earthquake Administration, Key Laboratory of Earthquake Engineering and Engineering Vibration, People's Republic of China

ARTICLE INFO

Keywords:

Site classification
Horizontal-to-vertical (H/V) spectral ratio
National Strong Motion Observation Network System (NSMONS)
Strong motion station
KiK-net data

ABSTRACT

Reliable site classification of the stations of the China National Strong Motion Observation Network System (NSMONS) has not yet been assigned because of lacking borehole data. This study used an empirical horizontal-to-vertical (H/V) spectral ratio (hereafter, HVSR) site classification method to overcome this problem. First, according to their borehole data, stations selected from KiK-net in Japan were individually assigned a site class (CL-I, CL-II, or CL-III), which is defined in the Chinese seismic code. Then, the mean HVSR curve for each site class was computed using strong motion recordings captured during the period 1996–2012. These curves were compared with those proposed by Zhao et al. (2006a) for four types of site classes (SC-I, SC-II, SC-III, and SC-IV) defined in the Japanese seismic code (JRA, 1980). It was found that an approximate range of the predominant period T_g could be identified by the predominant peak of the HVSR curve for the CL-I and SC-I sites, CL-II and SC-II sites, and CL-III and SC-III + SC-IV sites. Second, an empirical site classification method was proposed based on comprehensive consideration of peak period, amplitude, and shape of the HVSR curve. The selected stations from KiK-net were classified using the proposed method. The results showed that the success rates of the proposed method in identifying CL-I, CL-II, and CL-III sites were 63%, 64%, and 58% respectively. Finally, the HVSRs of 178 NSMONS stations were computed based on recordings from 2007 to 2015 and the sites classified using the proposed method. The mean HVSR curves were re-calculated for three site classes and compared with those from KiK-net data. It was found that both the peak period and the amplitude were similar for the mean HVSR curves derived from NSMONS classification results and KiK-net borehole data, implying the effectiveness of the proposed method in identifying different site classes. The classification results have good agreement with site classes based on borehole data of 81 stations in China, which indicates that our site classification results are acceptable and that the proposed method is practicable.

1. Introduction

Post-earthquake investigations and engineering practice both indicate that local site conditions have a profound effect on the ground motion characteristics and the seismic performance of engineering structures during strong ground shaking (Wood, 1908; Seed et al., 1988; Tsai and Huang, 2000). Local site response generally shows deamplification or amplification in different period ranges that can result in severe damage to buildings if the predominant period of those structures is close to the predominant period of site amplification. This phenomenon has been observed in several devastating earthquakes that have occurred recently in China, e.g., the 2013 Lushan M_s 7.0 earthquake (Ren et al., 2013), 2014 Ludian M_s 6.5 earthquake (Ji et al., 2014a), and 2014 Jinggu M_s 6.6 earthquake (Dai et al., 2015).

Considering the strong correlation between local site conditions and earthquake damage, it is important to classify building sites into different categories in the seismic codes. The most widely used site classification parameter is the time-averaged shear-wave velocity over the top 30 m of the soil deposit (V_{S30}), as suggested by the NEHRP (Building Seismic Safety Council (BSSC), 2003) and Eurocode 8 (European Committee for Standardization (CEN), 2004). Several methods were developed to predict V_{S30} considering the surface geological profile or topography slope as a proxy of V_{S30} (Wills et al., 2000; Lee et al., 2001; Wald and Allen, 2007; Allen and Wald, 2009). These methods are generally used for estimating the overall V_{S30} distribution covering a relatively wide region rather than for a site-specific estimation, especially work well for where high slope contrasts could be observed such as mountain and basin areas. Another effective way is based on an

^{*} Corresponding author at: No. 29 Xuefu Road, Harbin, Heilongjiang 150080, People's Republic of China.

E-mail addresses: JKingN@hotmail.com (K. Ji), renyefei@iem.net.cn (Y. Ren), ruizhi@iem.net.cn (R. Wen).

¹ Present address: 817 Ave Dollard, Outremont, Montreal, Quebec H2V 3G8, Canada.

² Present Address: No. 29 Xuefu Road, Harbin, Heilongjiang 150080, People's Republic of China.

empirical extrapolation relationship between V_{S30} and the time-averaged shear-wave velocity over the top soil shallower than 30 m (Boore, 2004; Kuo et al., 2012). However, due to limited drilling borehole data, this method is not practical for estimating V_{S30} of the sites of strong motion stations in China.

Following the rapid development of observation technology, strong motion recordings have been collected in many countries. Site classification of strong motion stations has an important role in the application of these recordings for seismic zonation, seismic hazard evaluation, and computation of seismic structural response. For instance, in ground motion prediction equations (GMPEs), even for similar magnitudes and distances, variations due to different site conditions can be considerable and must be properly taken into account (Takahashi et al., 2000). The parameter V_{S30} is commonly used in characterizing the site effect term in modern GMPEs, such as the Next Generation of Attenuation (NGA) models. However, for some strong motion stations the values of V_{S30} might be unavailable and therefore, their classification based on the predominant period of the site could be an affordable alternative (e.g., Zhao et al., 2006b; Alessandro et al., 2012).

The National Strong Motion Observation Network System (NSMONS) of China has been in formal operation since 2008, and a large number of high quality strong motion recordings have been obtained in recent years. However, most NSMONS station sites are classified only approximately as “rock” or “soil” because of lacking borehole data, which seriously limits the application of their data in GMPEs and other studies. To overcome a similar problem, an alternative to the V_{S30} -based site classification method was proposed by Zhao et al. (2006a), based on the curves of the horizontal-to-vertical (H/V) spectral ratio (hereafter, HVSR) of strong motion recordings. This site classification method has been used in strong motion observation networks in many countries, e.g., Japan, Italy, and Iran (Zhao et al., 2006a; Alessandro et al., 2012; Fukushima et al., 2007; Ghasemi et al., 2009). For the NSMONS, Wen et al. (2010, 2011) classified near-fault stations in the Wenchuan earthquake using both the HVSR and the response spectral shapes method. Ji et al. (2014b) performed similar work for near-field stations in the 2013 M_s 7.0 Lushan earthquake. Their classification results had good correlation with the borehole data of some stations, which demonstrated the practicability and efficiency of the methods. Wen et al. (2014) classified temporary stations within this region using a new classification scheme proposed to improve the reliability of the HVSR method. All of these earlier studies focused on triggered stations in one earthquake event rather than all the stations of the NSMONS network. Besides, the stations were all classified according to the classes defined in the Japanese seismic design code for highway bridges (Japan Road Association (JRA), 1980), corresponding to four empirical HVSR curves suggested by Zhao et al. (2006a). Therefore, it is necessary to develop empirical curves associated with the site classes defined in the Chinese seismic code and to classify all the strong motion stations that comprise the entire observation network.

In this study, site characteristics of selected strong motion stations of KiK-net in Japan were investigated, and the corresponding mean HVSR curves for each site class, as defined in the Chinese seismic code, were computed. An empirical site classification scheme was proposed to increase the success ratio. The applicability of the proposed scheme was verified using the same KiK-net dataset and borehole data of selected NSMONS stations. Finally, based on strong motion recordings obtained during 2007–2015, 178 NSMONS stations (with recordings of at least three earthquake events) were classified using the proposed classification scheme and schemes developed in other studies.

2. Empirical H/V curve for different site classes

2.1. Site class definitions for Chinese seismic code

The H/V technique was first proposed by Nakamura (1989) who used a horizontal-to-vertical Fourier spectrum ratio of ground microtremors to

Table 1

Site class definitions used in the study by Zhao et al. (2006a) for Japanese sites and the approximately corresponding NEHRP site classes (BSSC, 2003).

Site class	Site predominant period	Average shear-wave velocity	NEHRP class
SC I: (rock/stiff soil)	$T_g < 0.2$ s	$V_{S30} > 600$ m/s	A + B + C
SC II: (hard soil)	$0.2 \text{ s} \leq T_g < 0.4$ s	$300 \text{ m/s} < V_{S30} \leq 600$ m/s	C + D
SC III: (medium soil)	$0.4 \text{ s} \leq T_g < 0.6$ s	$200 \text{ m/s} < V_{S30} \leq 300$ m/s	D
SC IV: (soft soil)	$T_g \geq 0.6$ s	$V_{S30} \leq 200$ m/s	D + E

Note: T_g means the site’s predominant period.

evaluate site characteristics. Later, Yamazaki and Ansary (1997) applied this method in earthquake ground motions. Zhao et al. (2006a) proposed an empirical site classification method based on the mean spectral ratio of earthquake recordings for strong motion stations in Japan. The definitions of site class criteria were based on the Japanese seismic design code for highway bridges (JRA, 1980). The ranges of the predominant period T_g for each site class, and the ranges of V_{S30} and the corresponding NEHRP site classes (BSSC, 2003) are listed in Table 1.

Unlike the definitions in the Japanese design code and the NEHRP, the four class categories defined in the Chinese seismic code (GB50011-2010) (MHURC, 2010) are defined by two parameters: the 20-m average shear wave velocity (V_{S20}) and the thickness of the soil layers (H) above the engineering bedrock layer where $V_s \geq 500$ m/s, as shown in Table 2. Noting that I_0 is a subclass of I. The value of 500 m/s was originally used to represent stiff soil or rock, including stable rock and dense detritus in previous 1989 version of Chinese seismic code. It was derived from a statistical analysis of a large number of S-wave velocity data of rock and dense detritus in the Chinese mainland. It has been treated as a representative of engineering bedrock in Chinese seismic code till now. Furthermore, 20 m is shallower than the value of 30 m associated with the commonly used parameter V_{S30} and the additional index H characterizes different site effects for the same V_{S20} range. Because of the differences in the site class definitions between the two codes (i.e., Tables 1 and 2), the four HVSR mean curves given by Zhao et al. (2006a) might not be suitable for the Chinese code. Therefore, the first objective of this study was to develop an empirical HVSR curve for each site class in the Chinese code.

The HVSR method has been validated estimating the similar predominant period with other methods, such as the spectral ratio method of reference site and some inversion methods. But the predominant period could not be used as the only index for site classification because the soil layer thickness (represented by H in Chinese seismic code) could also impact the HVSR amplitude. Considering the amplitude of site response determined by HVSR method is not accurate, or not consistent with other methods (Bonilla et al., 1997; Lermo and Chávez-García, 1993; Kuo et al., 2015), we chose the SI index proposed by Ghasemi et al. (2009) to distinguish different site classes. It could measure the extent of the similarity of relative H/V curve shape rather than absolute amplitude. The second objective of this study was to

Table 2

Definitions of site classes in the Chinese seismic code (GB50011-2010) (MHURC, 2010).

20 m equivalent shear wave velocity V_{S20} / (m s^{-1})	Thickness of soil layer H^* /m				
	I_0	I	II	III	IV
> 800	0				
(500, 800]	0				
(250, 500]		< 5	≥ 5		
(150, 250]		< 3	3–50	> 50	
≤ 150		< 3	3–15	15–80	> 80

H^* : thickness of soil layer above rock with $V_s \geq 500$ m/s.

propose a classification procedure considering both the predominant period and the shape of HVSR curve. Hereafter, class CL-I refers to the combination of I_0 and I, and classes CL-II, CL-III, and CL-IV refer to II, III, and IV, respectively.

2.2. KiK-net strong motion dataset

As mentioned in the introduction, because of the lack of borehole data, NSMONS stations are classified simply as “rock” and “soil”; therefore, the mean HVSR curve for each class cannot be computed directly using these data. The ground motion recordings used in this study, extracted from the Japanese KiK-net dataset (1996–2012), comprised 151,731 groups of triaxial records from 609 triggered stations. Apart from the large number of recordings, another important advantage of KiK-net is that the borehole depths reach rock layers where the shear wave velocity far exceeds 500 m/s. K-net stations in Japan have also captured many recordings; however, their borehole depths extend to only 20 m, which can result in classification failure for soft sites (e.g., CL-III and CL-IV sites) for which the value of H is usually > 20 m (see Table 2). Thus, data from K-net were not used in this study.

Of the 609 triggered stations, 94 were classified as CL-I, 482 were classified as CL-II, 29 were classified as CL-III, and only 4 were classified as CL-IV according to the criteria presented in Table 2. Thus, CL-II stations account for nearly 80% of the total, which reflects the relatively wide range of values of V_{S20} and soil thicknesses shown in Table 2. On the Chinese mainland, CL-II sites cover most regions of the country, and they are regarded as reference sites for the calculation of ground motion parameters in seismic zonation mapping.

Site classification in the Chinese seismic code depends not only on the value of V_{S20} but also on the value of H . A slight change in the boundary data of V_{S20} and H could cause the classification result to “jump” from one class to another. If the possibility of uncertainty in the measurement of borehole data were considered, this phenomenon could be prevalent and should not be ignored. To prevent its impact spreading into the computation of the mean HVSR curve for each site class, we reduced the upper boundaries of V_{S20} and H by 15% and increased the lower boundaries by 15%. The major adjustment focuses on the boundary of the CL-II class of sites because this class comprises 80% of the total number and it could overwhelm the other site classes. Because of the large number of recordings and stations in KiK-net, there is no need for concern that adjustment of the boundaries might cause data insufficiencies. The new classification boundaries, shown as shaded areas in Fig. 1, effectively solve the problem of mixed-boundary data mentioned before and yet, still guarantee the selection of a certain number of stations. It is worth noting that the CL-IV sites refer to

extremely soft soil conditions with sedimentary layers more than 80-m thick; areas that are actually unsuitable for the placement of a strong motion station according to the related regulations in China. Even in KiK-net, there are only four stations classified as CL-IV sites. Therefore, the mean HVSR curve for CL-IV sites was not calculated in this study.

To obtain a stable curve of the mean HVSR, stations triggered in at least five earthquakes were selected. In fact, almost every station can fulfill this requirement because of the high density of the KiK-net stations and high frequency of occurrence of earthquakes. In this study, a fourth-order acausal Butterworth filter was used to remove noise contamination, especially in the long-period part. The corner frequency for the high-pass and low-pass filters was selected as 0.25 and 25.00 Hz, respectively, sufficient for the target period range of the spectral ratio curve of 0.05–3.0 s.

Another two important problems that require consideration are soil nonlinearity and the signal-to-noise ratio (SNR). The soil nonlinearity phenomenon is often observed in many large earthquake events, and it could influence the shape of the HVSR curves because of the drift of the predominant period and de/amplification of the spectral ratio. Based on studies by Wen et al. (2006) and Ji et al. (2014c), recordings with peak ground acceleration (PGA) of > 100 Gal are more likely to be influenced by soil nonlinearity. To avoid possible large variation in the HVSR curves, attributable to soil nonlinearity, only those recordings with PGA of < 100 Gal were selected in this study. The SNR is another factor that might influence the spectral ratio curve in the long-period part, and low SNR recordings are often captured in relatively small earthquakes. Therefore, recordings with PGA of < 5 Gal were excluded in this study to avoid the possibility of poor-quality signals (Ghasemi et al., 2009).

The recordings were processed and selected to meet the above requirements, and 279 stations were classified according to the definitions of site classes in the Chinese seismic code (Table 2). The locations of the CL-I, CL-II, and CL-III sites are distinguished by different marks in Fig. 2, and the numbers of stations and recordings for each site class are listed in Table 3.

2.3. Empirical mean HVSR curves for the Chinese seismic code

The 5% damped H/V velocity response spectral ratio was calculated for each recording instead of the traditional H/V ratio of the Fourier amplitude spectrum. This was undertaken because of the high computation efficiency and consistent smoothing achieved in the response spectral ratio for all recordings when the same damping ratio is used (Zhao et al., 2006a). Consequently, the geometric mean HVSR curve for each site class was obtained, as shown in Fig. 3 (except CL-IV). The curve for the CL-I class of sites is flatter than CL-II and CL-III with

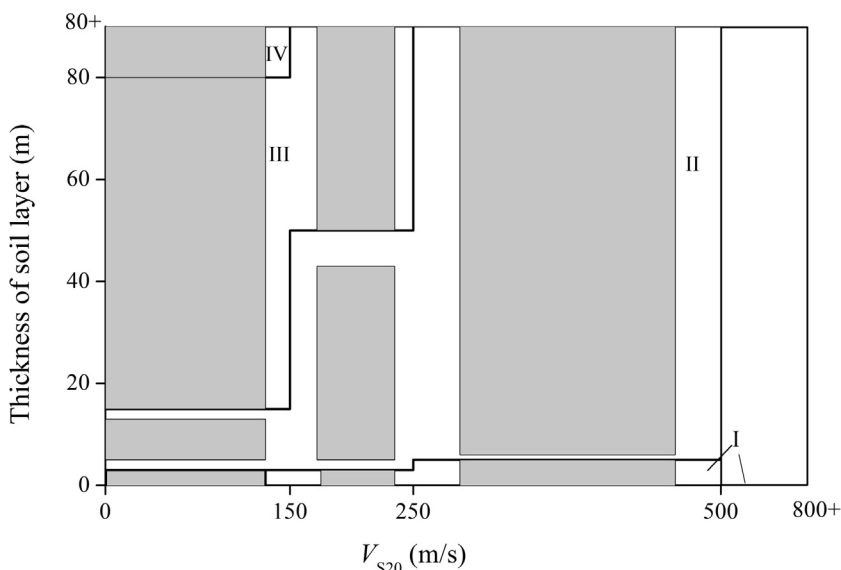


Fig. 1. Range of V_{S20} and thickness of soil layer for each site class defined in the Chinese seismic code. Dark black lines indicate the original boundaries between different classes; shaded areas indicate the new range for each class after reducing or increasing the boundary values.

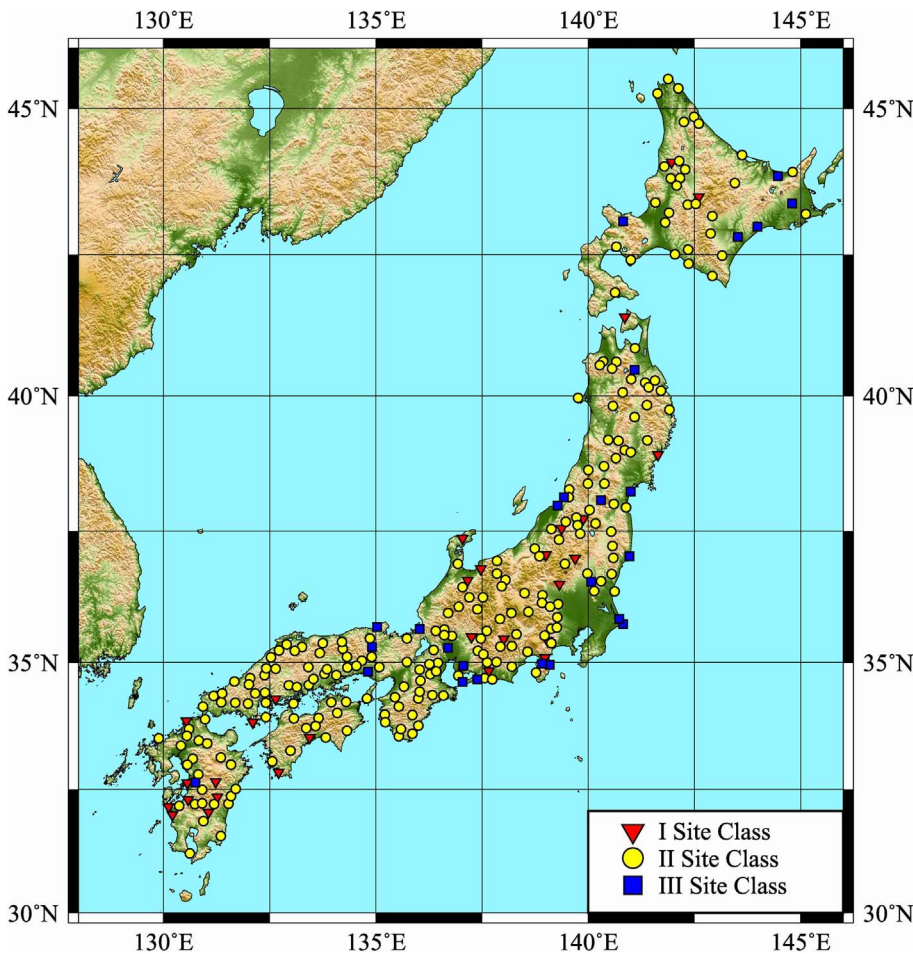


Fig. 2. KiK-net sites used in this study and their site classes assigned according to borehole data.

Table 3
Numbers of studied stations and recordings for each site class in KiK-net.

Site classes	No. of stations	No. of recordings	Per. of the stations (%)	Per. of the recordings (%)
I	30	3341	11	9
II	223	29913	79	83
III	26	2764	10	8

amplitude around 2.0. The curve for the CL-II class of sites has peak periods of 0.15–0.45 s with amplitude near 2.75. It should be noted that there is only one peak for both CL-I and CL-II but two peaks for CL-III at periods of 0.3 and 0.9 s. It shows the difficulty of classifying sites based on the Chinese code simply using the range of T_g identified as the peak period of the HVSR curves.

The HVSR curves of the four classes calculated by Zhao et al. (2006a) show a remarkable predominate period range for each class (Fig. 3(d)), which is consistent with that proposed by the JRA (1980) (see Table 1). The classification scheme of the Chinese seismic code depends not only on V_{S20} but also on the thickness of the soil layer H ; therefore, the T_g range is relatively fuzzy. The shapes of the H/V curves for CL-I and CL-II are similar to SC-I and SC-II, respectively, but they are flatter in the long-period range. The CL-III class of sites is equivalent to the combination of the SC-III and SC-IV classes because the double predominant periods (0.3 and 0.9 s) of the CL-III class of sites are close to the individual predominant periods of the SC-III (0.4 or 0.5 s) and SC-IV (0.8 s) classes.

The standard deviations at different periods for each class of sites are also shown in Fig. 3. The values are relatively higher for the range of periods < 0.15 s, reaching the average level of 0.5 for all three site classes. For periods > 0.15 s, the value reduces with increased period

and it reaches close to 0.25 after 1.00 s. The response of longer period is more related to deeper soil velocity structure, so the variance does not vary a lot compared to shallow structure which results in big response variance in the short period response. This phenomenon is also observed for H/V curves in the study of Zhao et al. (2006a) as shown in Fig. 3(d). The standard deviation of CL-III is a little higher than the other two classes, which might be related to the relatively small number of stations of this class. The entire range of standard deviations is similar to previous studies: 0.25–0.55 (Zhao et al., 2006a), 0.40–0.65 (Fukushima et al., 2007), around 0.59 (Ghasemi et al., 2009). The feature of relatively low standard deviations at moderate and long periods implies that significant and stable differences exist within the shapes of the HVSR curves among these three classes of sites.

The ranges of the predominant period of the three site classes defined in the Chinese seismic code can be evaluated approximately by their mean HVSR curves (Fig. 3(a)) as $T_g \leq 0.15$ s for CL-I sites, $0.15 < T_g \leq 0.45$ s for CL-II sites, and $T_g > 0.45$ s for CL-III sites. The T_g ranges for different site classes are compared with those proposed by the JRA (1980) in Fig. 4. Generally, there is an approximate one-to-one correspondence between the CL-I, CL-II, and CL-III classes and the SC-I, SC-II, and SC-III + SC-IV classes, respectively. Lü and Zhao (2007) and Guo (2010) evaluated the approximate V_{S30} ranges of the site classes defined in the Chinese seismic code using borehole data from Taiwan, Japan, the U.S.A., and some other regions. Compared with the definitions in the JRA (1980) (see Table 1), an approximately similar range of V_{S30} values can be observed for each site class between the two codes, as shown in Fig. 4(b), which links to the consistency of the T_g range mentioned above.

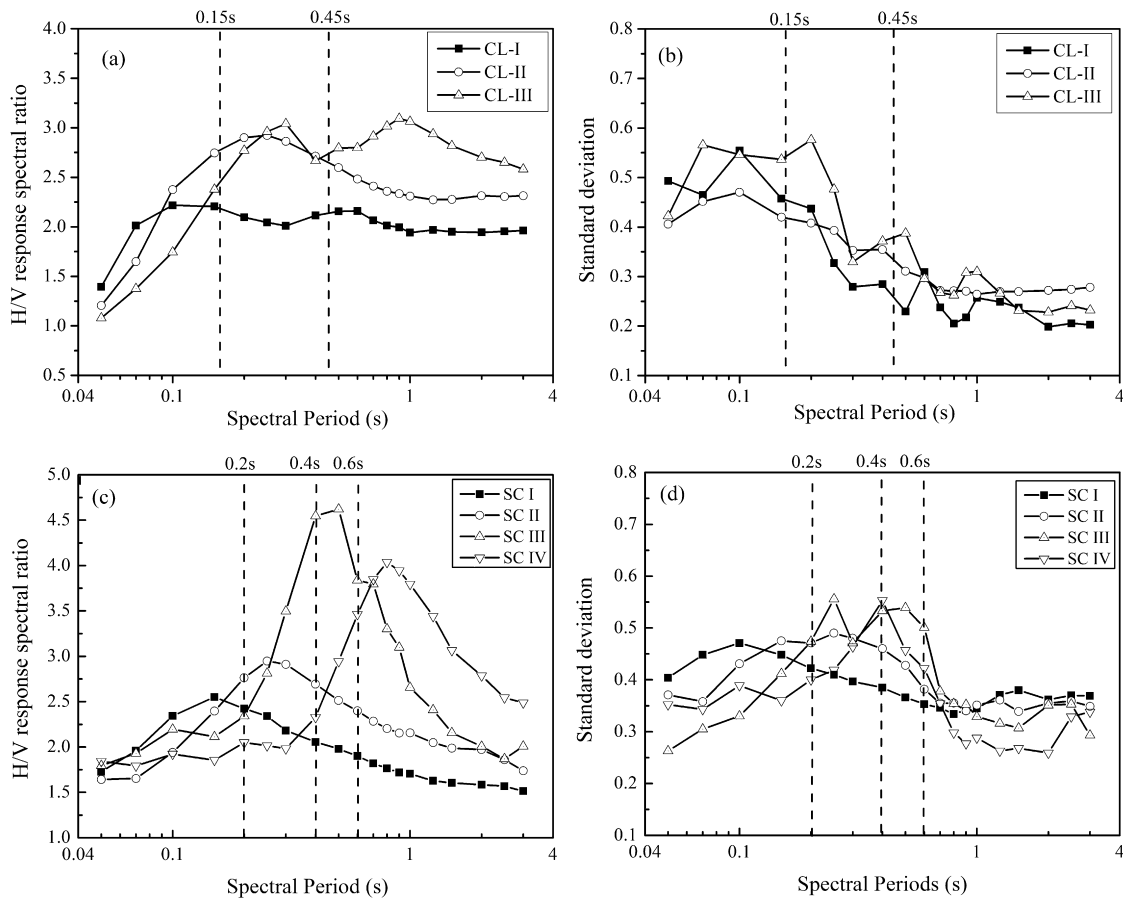


Fig. 3. (a) Mean HVSR curves and (b) corresponding standard deviations proposed by this study for three site classes defined in the Chinese seismic code; (c) mean HVSR curves and (d) corresponding standard deviations proposed by Zhao et al. (2006a) for the four site classes defined in the JRA (1980).

3. Empirical site classification scheme

3.1. Different empirical site classification methods

(1) Method proposed by Zhao et al. (2006a)

In earlier years, the first dominant peak of the HVSR curve was taken as the predominant period of the site, and it was compared with the corresponding period ranges in the JRA (1980) to classify the sites. However, this method might fail in some special cases. For example, for many relatively hard sites, it is usually not possible to discern the exact

peak of the HVSR curves because of their overall flat shape, especially when the number of records is small. Therefore, high success rates were generally not expected when using this method.

To overcome this problem, Zhao et al. (2006a) proposed an automatic classification based on the probabilistic distribution of spectral ratios and they designed a site classification index (SI) as follows:

$$SI_k = \frac{2}{n} \sum_{i=1}^n F(-\text{abs}[\ln(\mu_i) - \ln(\bar{\mu}_{ki})]) \quad (1)$$

where k is the site class number, n is the total number of periods, $F()$ is the normal cumulative distribution function, μ_i is the mean H/V

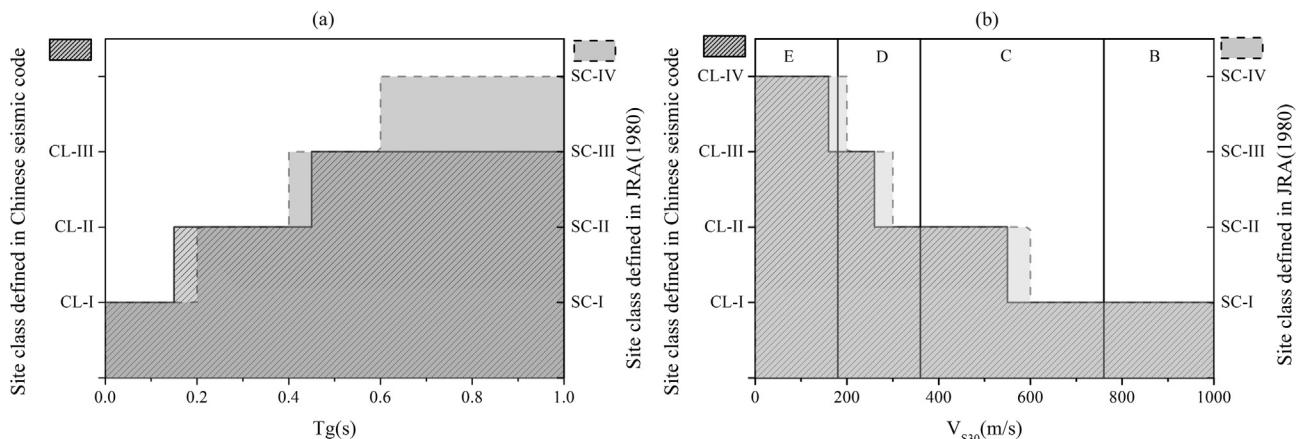


Fig. 4. Comparisons of predominant period range (a) and V_{s30} range (b) between the site classes defined in the Chinese seismic code and the JRA (1980). Corresponding ranges for the NEHRP site classes B, C, D, and E are also shown.

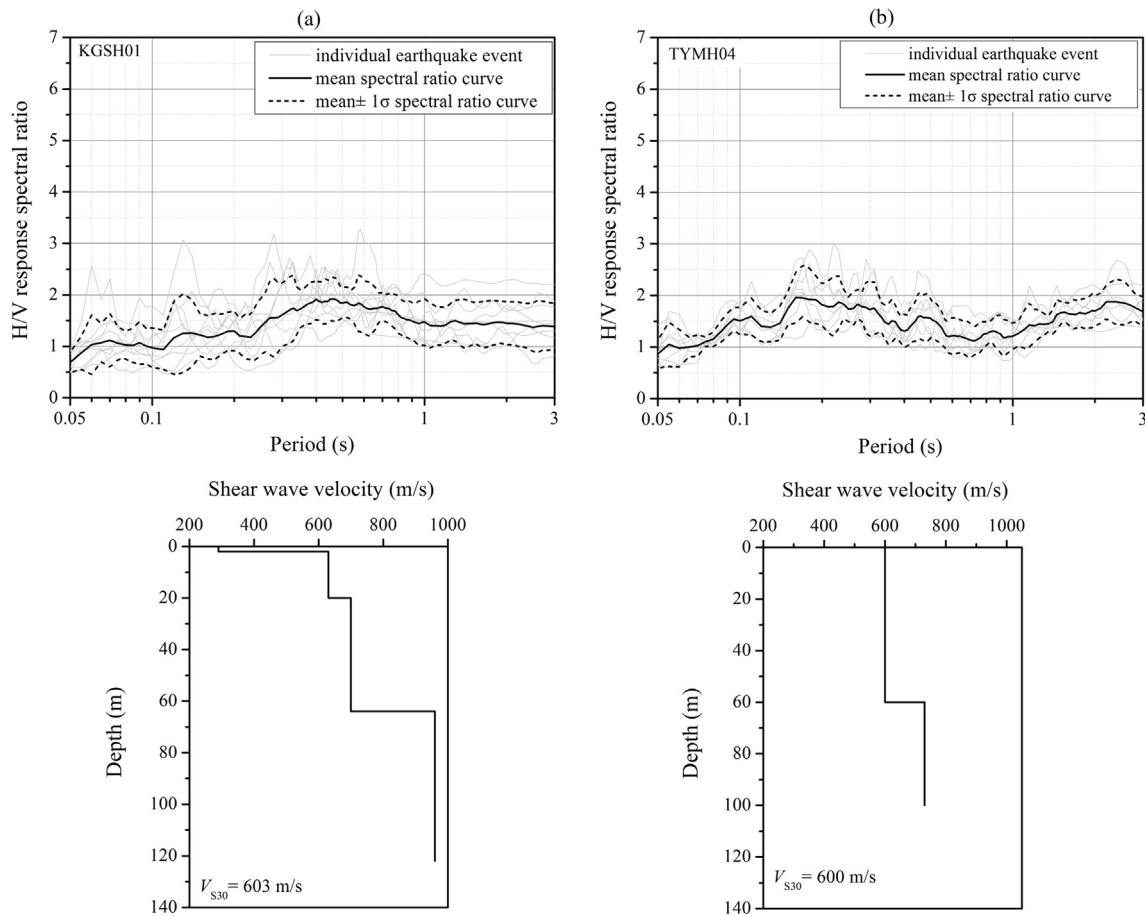


Fig. 5. Mean H/V spectral ratio curves and borehole profiles for two KiK-net stations: (a) KGSH01 and (b) TYMH04.

spectral ratio of the target site for the i -th period, and $\bar{\mu}_{ki}$ is the mean H/V spectral ratio for the k -th site class averaged over all sites of the dataset for the i -th period. We call $\bar{\mu}_{ki}$ as the standard HVSR hereafter in this study to distinguish it with μ_i . This method considers the differences of the HVSRs for all periods. The value of SI is calculated for each site and the one with the largest value is assigned to this site class. It is effective for sites of the SC-I, SC-III, and SC-IV classes, but it has a low success rate for SC-II sites (Zhao et al., 2006a).

(2) Method proposed by Ghasemi et al. (2009)

As Zhao’s method focuses only on the absolute difference of all the periods, it cannot always identify the extent of the similarity in the shapes of the curves effectively, supposing in a particular situation that one curve just drifts upwards from the original location. These two completely “similar” curves could not be identified by the method of Zhao et al. (2006a), which might cause incorrect classifications in practice. Ghasemi et al. (2009) proposed a site classification index to improve the accuracy of Zhao’s method, as follows:

$$SI_k = 1 - 6 \sum \frac{d_i^2}{n(n^2 - 1)} \tag{2}$$

where d_i is the difference between each rank of corresponding values of the standard HVSR curves for the k -th site class and the target sites, and n is the total number of periods. The proposed parameter SI_k is actually the Spearman’s rank correlation coefficient (Spearman, 1904), which is a nonparametric rank proposed as a measure of the degree of association between two variables. In this context, it is used to measure the correlation between the target and standard HVSR curves. The range of Spearman’s correlation coefficient is -1 to 1 , and a value equal to 1

would indicate perfect correlation between the two curves. The larger the value of SI, the greater the similarity between the shapes of the two curves.

3.2. Special situations in matching HVSR curves

Although the two empirical methods mentioned above have been applied in many countries or regions, e.g., Japan, Iran, Italy, and Taiwan, high rates of success are not always expected for each site class. The main problem in the step of matching the HVSR curves derives from the fact that the site responses at different stations are rather varied and complex, and some special situations that could interfere with the classification results should be considered.

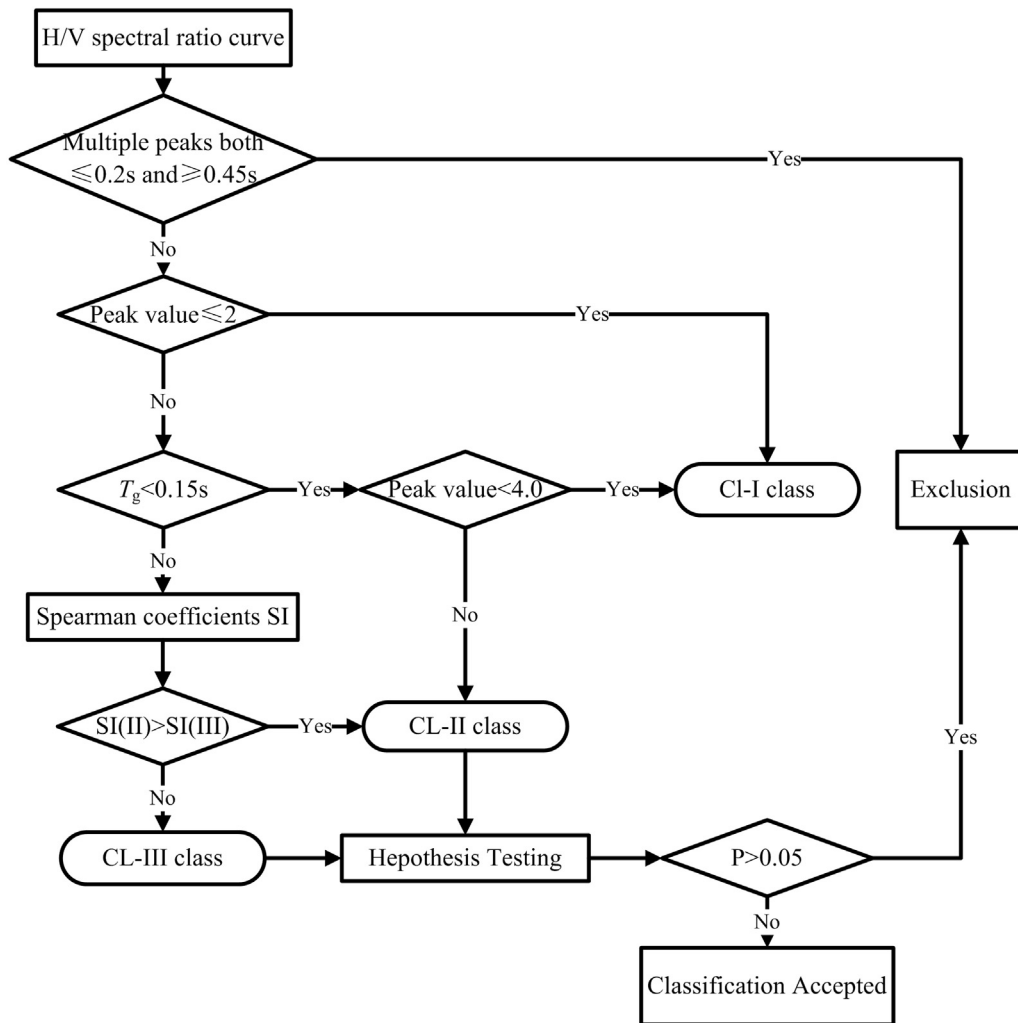
(1) Head–tail joggling

The head–tail joggling phenomenon was first observed by Wen et al. (2011). It means that the weight of matching an HVSR curve at a non-predominant period (usually at short and long periods, i.e., the head and tail of the HVSR curve) is overestimated. It might equivalently decrease the weight around the predominant period (i.e., T_g), leading to the possibility of incorrect classification. Therefore, a method was proposed to assign individual weights at each period automatically using the entropy weight theory (Wen et al., 2011). A scenario test case showed that the proposed method could effectively avoid the effect of head–tail joggling on the final classification result.

(2) Flat H/V curve

For rock/stiff soil sites, the HVSR curve might be relatively flat with no predominant peak, i.e., the value of T_g is indeterminable. As shown in Fig. 5,

Fig. 6. Flowchart of proposed empirical site classification scheme for NSMONS stations.



the mean HVSR curve of two KiK-net stations with shear wave velocity of > 600 m/s is almost flat over the entire period range. This type of curve could not be classified by the range of T_g and it might also fail with the previously mentioned site classification methods. Alessandro et al. (2012) defined a new site class that refers to generic rock when the curve displays an almost flat HVSR (< 2.0) without a clear peak. A similar proposal was also offered by Wen et al. (2014) when they classified temporary strong motion stations based on the aftershocks of the Wenchuan earthquake.

(3) Multiple peaks

For some sites, more than one predominant peak period might be identifiable in the HVSR curve, and these sites are likely to be classified incorrectly by both of the above methods. One obstacle is the uncertainty in identifying an exact value of T_g . Another important problem is the difficulty of obtaining the best solutions for both Eqs. (1) and (2). The HVSR shapes of such sites are extraordinary because of their multiple peaks but only one peak for the standard curves in the study of Zhao et al. (2006a) (e.g., Fig. 3(c)). In previous studies, sites with this type of HVSR curve were usually excluded or classified into a newly defined class (Fukushima et al., 2007; Alessandro et al., 2012).

3.3. Proposed new site classification scheme

High rates of success are not always expected when using schemes based on the predominant period or the shapes of spectral ratio curves because of interference caused in some special situations, as in the three

cases mentioned above. In this study, an empirical site classification scheme was proposed that considers the peak period, amplitude, and shape of the HVSR curve, as shown in Fig. 6, the details of which are explained in the following.

- If a curve has more than one peak and if one (or more) of them lies within the range of short periods (< 0.20 s) while the other (or others) lies in the range of long periods (> 0.45 s), this site would be classified ambiguously; therefore, it should be excluded. This aims to avoid any interference in the classification of CL-I sites, some of which have a relatively small T_g . The set period range (0.20 s and 0.45 s) depends on the T_g boundary separating each site class, as shown in Fig. 3(a). The mean curve of CL-III sites has two peaks (i.e., 0.3 and 0.9 s). Therefore, if this type of site were excluded without consideration of its range of peak period, many stations would fail the classification process.
- When the amplitude of the HVSR is < 2.0 over the entire period range, the shape of the curve is recognized as relatively flat. The site can be classified directly as belonging to class CL-I. For a site with a flat curve, classification schemes using the SI index (Eqs. (1) and (2)) cannot perform well because of the head-tail joggling phenomenon, which is one of the primary factors that affect the success rates (Wen et al., 2011).
- When T_g is < 0.15 s, the site is classified as CL-II if the peak value is > 4.0 and as CL-I, if < 4.0 . This step recognizes that some CL-II sites might have a short predominant period similar to CL-I sites, but that their amplification is usually relatively higher. We selected

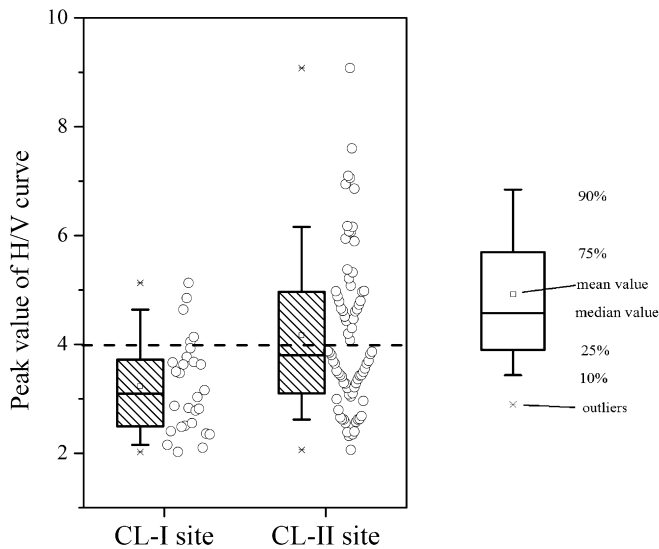


Fig. 7. Box-and-whisker plot for peak value of HVSR curve when $T_g < 0.15$ s.

all stations with $T_g < 0.15$ s in the KiK-net database and calculated the corresponding amplitudes for CL-I and CL-III classes, as shown in the box-and-whisker plot in Fig. 7. The H/V amplitude at T_g is < 4.0 for almost 80% of CL-I sites and > 4.0 for 50% of CL-II sites. Therefore, the value of 4.0 was set as the boundary for distinguishing CL-I and CL-II sites in cases where $T_g < 0.15$ s.

- (d) As mentioned above, the ranges of T_g for classes CL-II and CL-III partially overlap and the amplitudes of the HVSR curves are partially similar (see Fig. 3(a)). Therefore, these two classes cannot be classified based simply on their range of predominant period or amplitude. The method proposed by Zhao et al. (2006a) may be not able to effectively distinguish the relative difference between the HVSR curves of these two classes. In this study, for the situation of $T_g > 0.15$ s, the Spearman’s correlation coefficient SI (Eq. (2)) was chosen to distinguish CL-II and CL-III sites. Because CL-I sites are classified through steps (a) to (c), only two targeted classes remain under consideration in this step; thus, the Spearman’s correlation coefficient method would be most effective.
- (e) After identifying the CL-II and CL-III classes, the significance of the Spearman’s correlation coefficients must be checked using a t -distribution hypothesis test at the 0.05 significance level. The testing targets are the mean HVSR of target station and the standard HVSR curve for CL-II or CL-III. If the significant value P is > 0.05 , the classification result is considered unacceptable and the station excluded.

4. Verification of proposed classification scheme

Before applying the proposed scheme to classify the NSMONS stations in China, it was necessary to verify the success rate for the site classification of the KiK-net stations using this scheme. As discussed before, 79% of the selected KiK-net stations are assigned as CL-II sites based on borehole data. Therefore, if we directly calculate the total success rate for all stations, the weight derived from the CL-II sites would be sufficiently large to submerge the contributions from the CL-I and CL-III sites. Consequently, we cannot determine exactly whether this scheme is effective for CL-I and CL-III sites. In this study, for each class assigned by borehole data, we calculated the percentage of sites classified as the k -th class based on their HVSR curves P_k , as shown in Fig. 8.

$$P_k = \frac{N_{k,X}}{N_X} \quad (3)$$

where N_X means the total number of the CL- X sites assigned by borehole data, and X represents the Roman numeral I, II, or III. The values of N_I , N_{II} , and N_{III} are 30, 223, and 26 (see Table 3), respectively. Here, $N_{k, X}$ means

the number of CL- X sites classified as the k -th class by the HVSR method. If k is equal to X , then P_k represents the success rate for the k -th class when using the proposed classification scheme.

As indicated in Fig. 8, the mean success rates for all three classes are all around 60%, whereas the classifications of the KiK-net stations as CL-I, CL-II, and CL-III sites, using the proposed scheme are 63%, 64%, and 58%, respectively. Overall, 20% and 17% of CL-I sites are classified incorrectly as CL-II and CL-III sites, respectively; 25% and 8% of CL-II sites are classified incorrectly as CL-I and CL-III sites, respectively; 4% and 38% of CL-III sites are classified as CL-I and CL-II sites, respectively.

Hereafter, the classification scheme proposed in this paper is described as Method 1. The same KiK-net stations were also re-classified using the SI index proposed by Zhao et al. (2006a) (Eq. (1); hereafter, described as Method 2) and Ghasemi et al. (2009) (Eq. (2); hereafter, described as Method 3). Furthermore, the value of P_k for each class was also calculated, as shown in Fig. 8. For Method 2, CL-I and CL-III sites are classified properly with a success rate nearly as high as 70%; however, for the majority of stations (i.e., CL-II sites), the success rate is only 25%. A low success rate was also observed by Zhao et al. (2006a) when they classified SC-II KiK-net stations. Therefore, they suggested using borehole data as supplementary information to increase the success rate. The performance of Method 3 is relatively better for CL-II sites (success rate of 63%) than for CL-III (46%) and CL-I (33%) sites. A comparison of the results of the three methods shows that the scheme proposed in this paper has better performance and could be used for NSMONS stations because it can achieve high success rates for all three classes, especially class CL-II, which is the class to which most of the NSMONS stations are assigned.

To get a convincing success rate, the validation set of stations usually should be excluded from the calibration set, which means some of the stations (treated as validation set) might not be included for the use of averaging HVSR. But the CL-I and CL-III stations (only 30 and 26 stations) are not enough to extract validation group without influencing the stability of calibrated standard curve. Thus, the re-sampling technique was used to validate the success rates for our proposed method. Taking the CL-I stations as an example, we randomly extracted 10 stations from the total 30 stations. They were treated as validation group and the remaining 20 stations were used as calibration group. For CL-II stations, the number of validation stations could increase into 20 stations due to the large total number (i.e. 223). Then our proposed classification method was used for classifying the sites of 10 validation stations and the success rates were computed for different site classes. Repeat this procedure for 20 times, and then we would get 20 groups of success rate. We took the average rate of these 20 groups as the final validation results. As shown in Fig. 9, the average success rates for three site classes are all around 60%, with a mean value of 64%, 62% and 58%, which are similar to the results using all stations in Fig. 8(a).

The comparison between the three methods indicates that procedures (Methods 2 and 3) simply using one SI could not handle complex situations in site classification or in complex structure regions. Our proposed scheme is more effective than them because the values of T_g , the amplitude of HVSR, and shape of the HVSR curve are all considered comprehensively. Furthermore, the sites are classified systematically using different indices in multiple steps, as shown in Fig. 6, rather than in the whole procedure using the same index, as in Methods 2 and 3. Although one specific index may perform better in the identification of one site class, it usually causes that the success rates of the other two site classes are sacrificed as shown in Fig. 8(b) and (c). Even if we use another index to improve the success rates for the other two classes, the results are still not satisfactory because a large part of the stations have been wrongly assigned in the first step.

5. Site classification for NSMONS stations

5.1. Strong ground motion data set

The NSMONS over mainland China includes more than 1000 strong

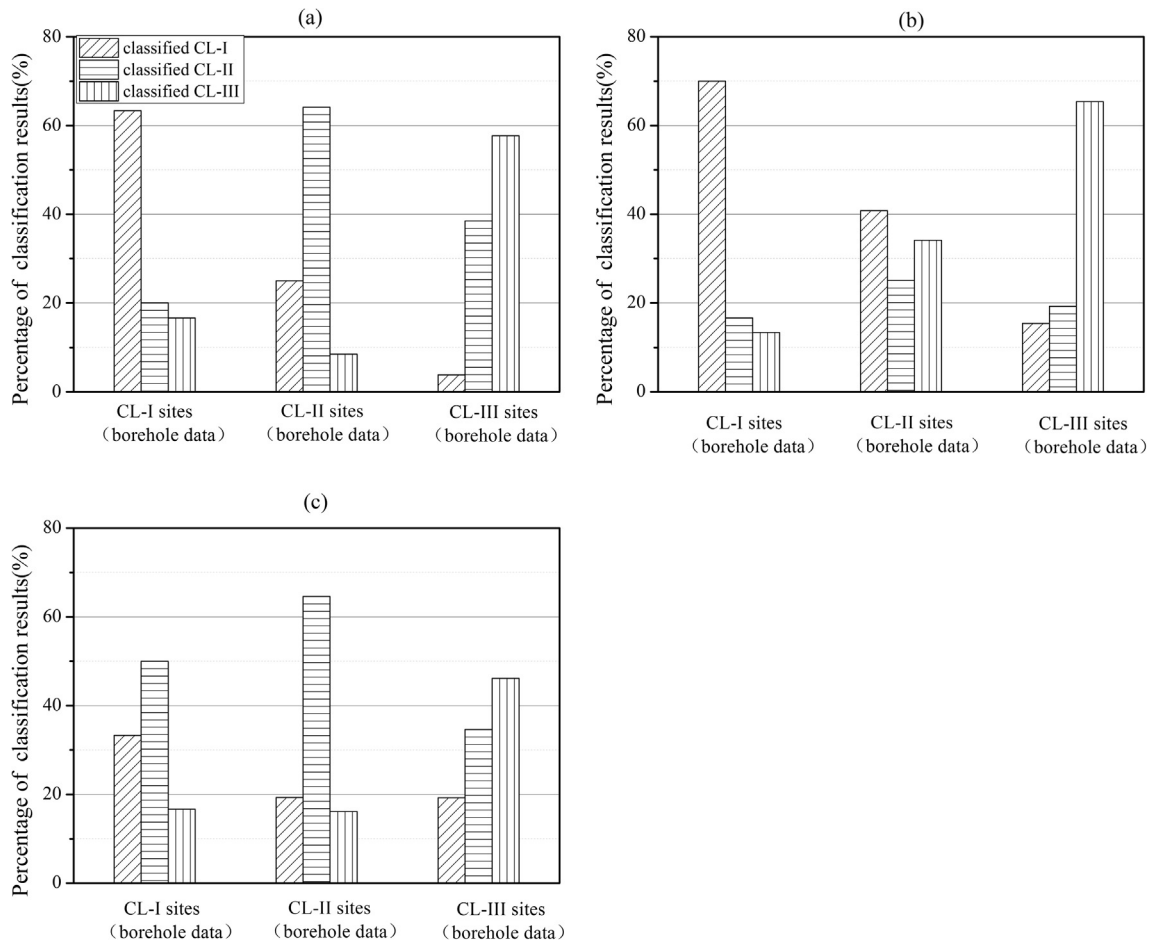


Fig. 8. Success rates of different site classification methods for Kik-net stations: (a) Method 1 proposed in this paper, (b) Method 2 proposed by Zhao et al. (2006a), and (c) Method 3 proposed by Ghasemi et al. (2009).

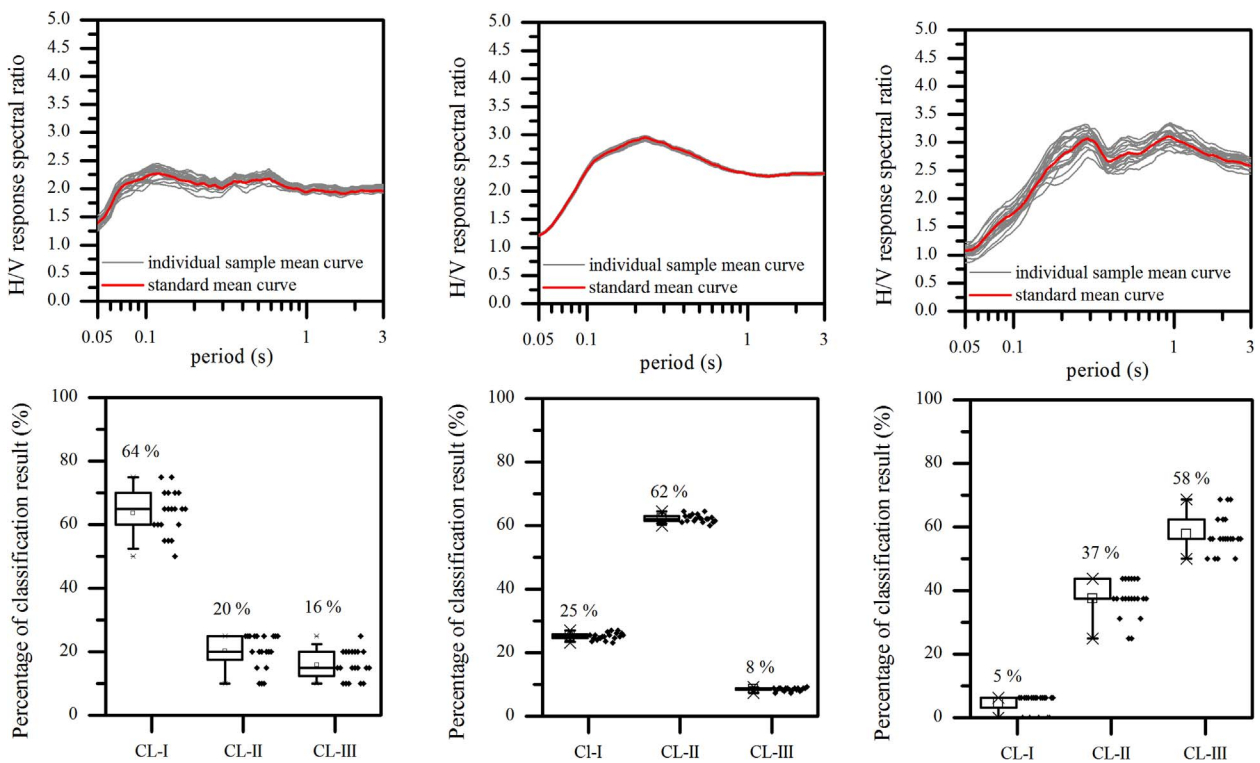


Fig. 9. Success rates of proposed site classification method for Kik-net stations using random sampling method.

motion stations distributed across most regions with high potential seismic hazard. The network began trial operation in early 2007 and formal operation commenced in March 2008. Just two months later, the network captured numerous recordings from the mainshock and aftershocks of the Wenchuan Earthquake (Li et al., 2008).

For this study, all seven published volumes of recordings from NSMONS, including 2007–2009, 2010–2011, and 2012–2013, and the mainshock and aftershock data of the Wenchuan and Lushan earthquakes were collated. The volume of recordings for 2014–2015 was incomplete and therefore, selected parts of the recordings including most of the typical destructive earthquakes, such as the 2014 M_s 6.5 Ludian earthquake, were used. Overall, 7183 recordings were collected and their magnitudes, geometric means of horizontal PGA, and distance distributions are shown in Fig. 10. Site classification work for some fixed and temporary stations using recordings from the Wenchuan and Lushan earthquakes has been completed in earlier work (Wen et al., 2011; Wen et al., 2014; Ji et al., 2014b), and therefore, the recordings obtained from the Wenchuan and Lushan earthquakes were excluded from this analysis. The recordings were processed using the procedure discussed in Section 2.2. A fourth-order acausal Butterworth filter was used with a bandwidth of 0.25–25.00 Hz. The PGA range was also set to 5–100 Gal. The data volume of the accumulated NSMONS recordings is not as large as the KiK-net dataset; therefore, stations with more than three recordings were selected for the computation of the mean H/V spectral ratio rather than those with five recordings. In regions without enough recordings, three recordings had been used as the threshold for H/V classification as in studies of Ghasemi et al. (2009) and Alessandro et al. (2012). To get stable and reliable mean curve, we have checked the recordings one by one and exclude the stations with obviously biased curves. Finally, 1281 recordings were selected for the computation, as shown in Fig. 10. A positive correlation between earthquake magnitude and epicenter distance is evident. According to previous studies (Yamazaki and Ansary, 1997; Zhao et al., 2006a), the spectral ratio variation between different magnitudes and distances is reasonably small, and this positive correlation was considered to have only a small adverse effect in this study.

5.2. Site classification results

Overall, 200 stations that met the above requirements were selected for site classification, and 178 of these were classified successfully using the scheme proposed in this paper. The other 22 were not assigned site classes because they satisfied one of the rules: multiple peaks or $P > 0.05$ (see Fig. 6). Of the 178 successfully classified stations, 14, 116, and 48 were classified as CL-I, CL-II, and CL-III, respectively. The geographical positions of all the classified and triggered NSMONS stations from 2007 to

2015 are shown in Fig. 11. There are more triggered stations and recordings in western regions of China because of the greater seismic activity in that area. Four regions are extracted and added geographic details to show the distributions of the site classes more clearly.

For region 01 located in Xinjiang Province, there are two large basins: Tarim Basin and Junggar Basin. For stations located in Junggar Basin, all were classified as CL-III sites, indicating a relatively soft soil profile. The stations located on the north edge of Tarim Basin are mostly classified as CL-II sites. The topography of west edge of Tarim Basin is relatively complex, including the basin, mountain, and plateau, so these stations are classified into three different sites. For region 03, the CL-II stations are mainly distributed in the edge of Sichuan Basin, and six CL-I stations are located in the mountain and plateau area. A relatively good correlation between site classification results and topography slope, as basin or mountain, could be observed in these two regions as shown in Fig. 11. The correlation is not obvious in region 04 due to its complex topography characteristics which consist of many mountains and hills with small rivers passing through.

The site classification results constitute a valuable asset for the scientific application of NSMONS recordings, e.g., the development of a regional GMPE where borehole data is limited. The GMPEs currently used in Chinese mainland are still using “soil” or “rock” as site terms due to a lack of borehole data. The site classification results provided by this study could be used as a representative of site term in GMPE as same as the study of Fukushima et al. (2007). Besides the classification results, the predominant period identified from HVSR curves could also be applied in GMPE studies, as in Italy and Japan (Alessandro et al., 2012; Zhao et al., 2006b; Zhao and Xu, 2013). Details of the site classification results are presented in Table A1 of the Appendix A.

The mean HVSR curves were computed for each site class based on the classification results of the NSMONS stations and then compared with those calculated using KiK-net data (see Fig. 3(a)), as shown in Fig. 12. Noting that for the mean HVSR curves calculated using KiK-net data, three site classes are classified according to borehole information. Overall, for each class, both curves have similar shapes and the same peak periods, indicating the practicability and effectiveness of our proposed scheme. The number of recordings from KiK-net used for calculating the mean HVSR curves was much greater than from NSMONS, implying the achieved mean curves are much smoother, especially around the peaks. This might explain why the peak values of the H/V curves derived using KiK-net data are slightly lower than from NSMONS data.

We collected borehole data from 81 stations and computed the V_{s20} to classify their site classes according to the definitions in the seismic code (Table 2), as shown in Fig. 13 and Table A1 of the Appendix A. Those data were collected from station construction reports which

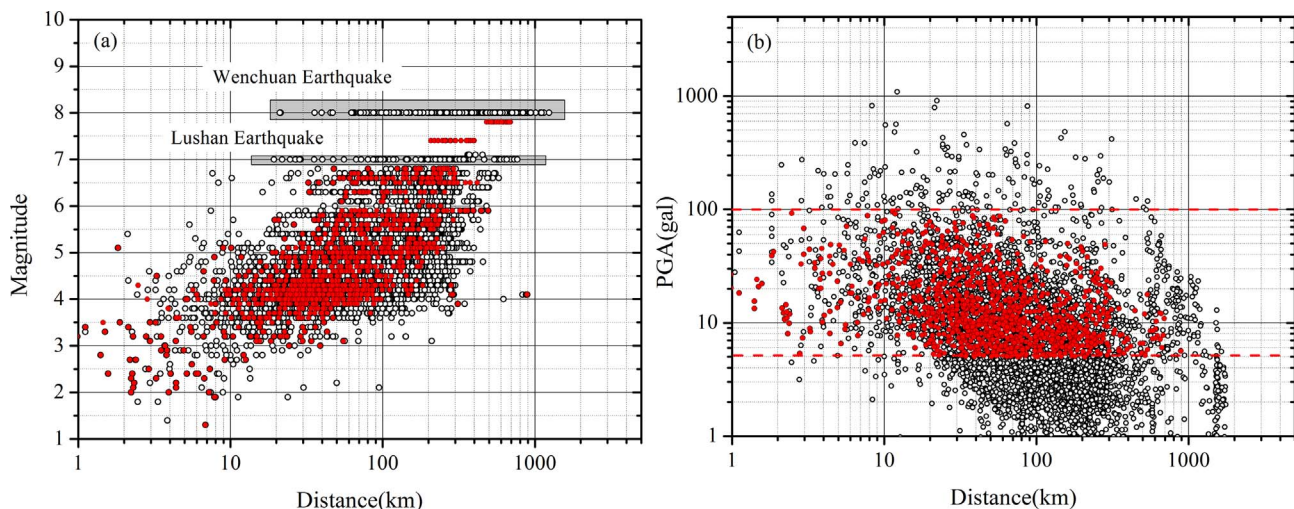


Fig. 10. (a) Magnitude vs. distance distribution and (b) geometric mean PGA for two horizontal components vs. distance. Red circles indicate finally selected recordings.

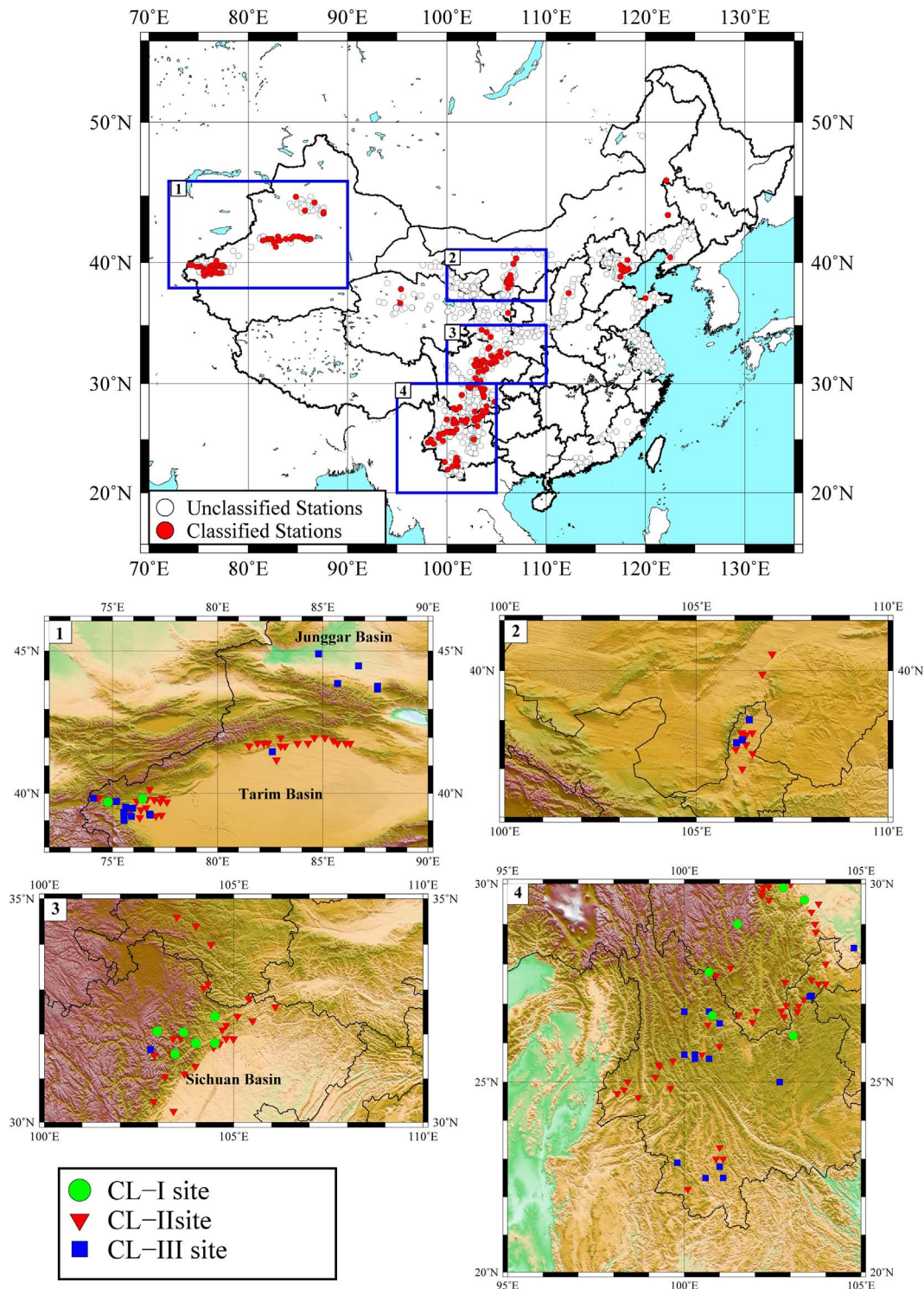


Fig. 11. Site classes proposed in this study for NSMONS stations.

provide the drilling P-S logging data of the soil layers. It can be seen that most stations are classified as the same site class whether using borehole data or the H/V spectral ratio of strong motion recordings. For CL-II sites, the proposed scheme has a success rate of almost 100% because of the large range of shear velocities and soil layer thicknesses defined for this class. However, for some stations, the boreholes were drilled to only 20, 30, or 50 m and the exact thicknesses (i.e., H) of their soil layer were not measured. These stations are plotted at the boundary of 20, 30, or 50 m, and their H values are presumed equal to 20, 30, or 50 m in Fig. 13. Therefore, the site classes of these stations might be

found to be CL-III rather than CL-II if the real H values could be achieved to more than 50 m.

It is worth noting that some stations with soil layer thicknesses of more than 80 or 50 m are located in the coastal area of Tianjin (i.e., 012DAT, 012DZZ, 012FTZ, 012GUG, 012XAZ, and 012ZHB). All these typical coastal soft soil sites were classified successfully as CL-III by the proposed method. Among the 14 stations classified as CL-I, only 5 had detailed borehole information. Two of these were classified successfully, but the other three were classified incorrectly because borehole data suggested they should be CL-II sites. It is because the depth of their

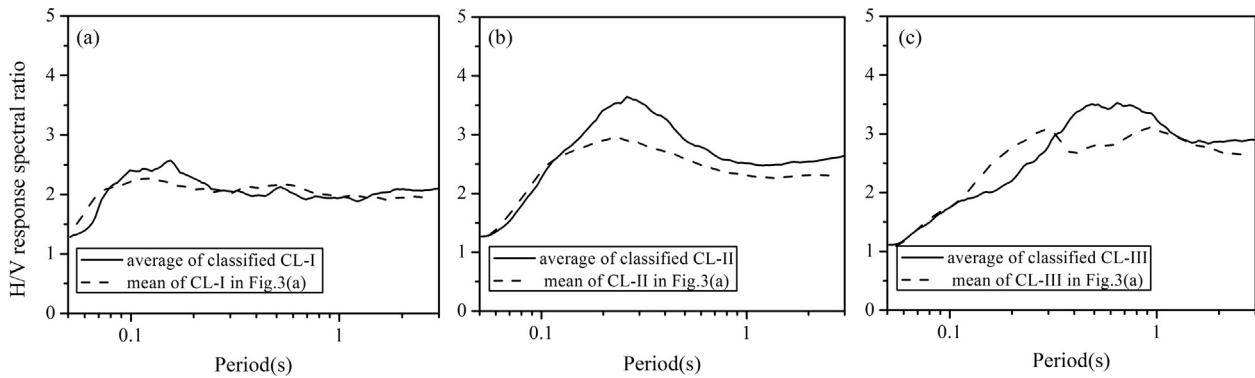


Fig. 12. Comparison between the mean HVSR curves derived from NSMONS data with those from KiK-net data: (a) CL-I sites, (b) CL-II sites, and (c) CL-III sites. The mean HVSR curves derived from KiK-net data are shown in Fig. 3(a).

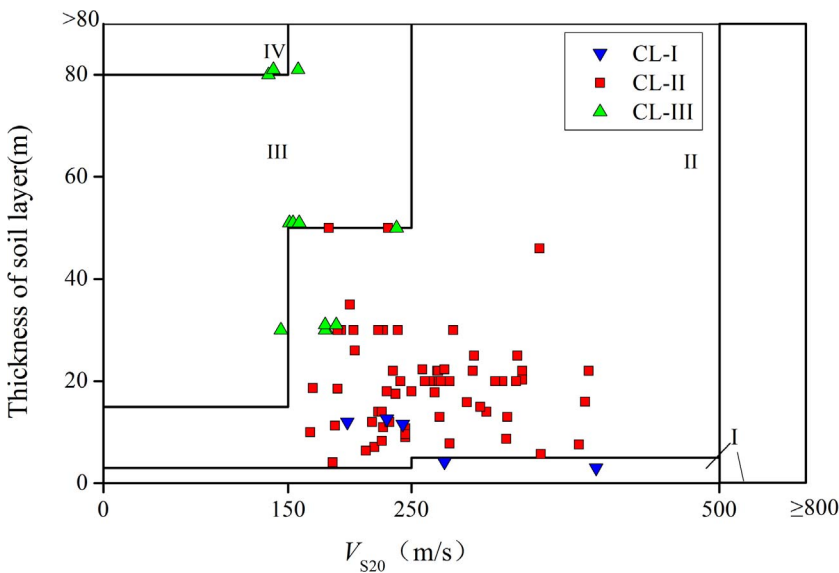


Fig. 13. Comparison of site classes based on borehole data and assigned by the H/V spectral ratio for some NSMONS stations.

relatively thin soil layer (nearly 10 m) is close to the boundary between CL-I and CL-II sites that this error could occur. Three other stations (051BCQ, 051MXD, and 065WSL) have no borehole data but be treated as “rock” sites according to the geological survey reports, which were accomplished during the time of selecting the station locations, and boreholes were not drilled at these sites. They were classified successfully as CL-I sites too. The comparison shown in Fig. 13 indicates the high success rates for site classification of NSMONS stations using the classification scheme proposed in this study.

5.3. Comparisons with other classification schemes

The selected NSMONS stations were also reclassified into four types of class: SC-I, SC-II, SC-III, and SC-IV using Methods 2 and 3. The classification results are listed in Table A1 of the Appendix A. The mean HVSR curve of each site class was re-computed based on these classification results and then compared with those standard curves given by Zhao et al. (2006a), as shown in Fig. 14.

For Method 2, the mean curves for both SC-I and SC-II are remarkably similar to the mean curves. However, a large difference exists for SC-III and SC-IV, indicating an unstable working mechanism of the classification index SI (Eq. (1)), especially for relatively soft sites. For Method 3, the mean HVSR curve is almost consistent with the standard curve for each of the four classes, except for a slight difference around the predominant peak period. This means that the Spearman’s rank correlation coefficient (Eq. (2)) could effectively identify the correlation of two HVSR curves and that it has good

performance in measuring the similarity of the shapes of the two curves. The Spearman’s correlation was checked using the same t -distribution hypothesis as in Section 3.3 for each station. The results show that five stations (051AXY, 051HYY, 051JZW, 051WCW, and 064NLG) are not acceptable at the 0.05 significance level and that Method 3 failed to classify them.

The numbers of stations for each site class were counted, and the results achieved by the different methods are compared in Table 4. The bold numbers indicate that most of the sites classified as CL-I by Method 1 were classified as SC-I by either Method 2 or 3; CL-II sites were classified as SC-II; and CL-III sites were classified as SC-III or SC-IV. This is consistent with the approximately similar ranges of T_g and V_{s30} for CL-I and SC-I, CL-II and SC-II, and CL-III and SC-III + SC-IV, as shown in Fig. 4.

6. Conclusions and discussions

The mean HVSR curves in the period range 0.05–3.0 s were computed for three site classes (CL-I, CL-II, and CL-III) defined in the Chinese seismic code, using 36,018 strong motion recordings and borehole data from 279 stations of Japan’s KiK-net. The predominant period T_g identified from three mean HVSR curve showed a range of < 0.15 s for CL-I sites, 0.15–0.45 s for CL-II sites, and > 0.45 s for CL-III sites, consistent with the range of SC-I, SC-II, and SC-III + SC-IV defined in the Japanese seismic code (JRA, 1980), respectively. CL-I and CL-II sites each had similar shapes to the HVSR curves of SC-I and SC-II given by Zhao et al. (2006a), respectively, and that class CL-III was similar to the combination of classes SC-III and SC-IV.

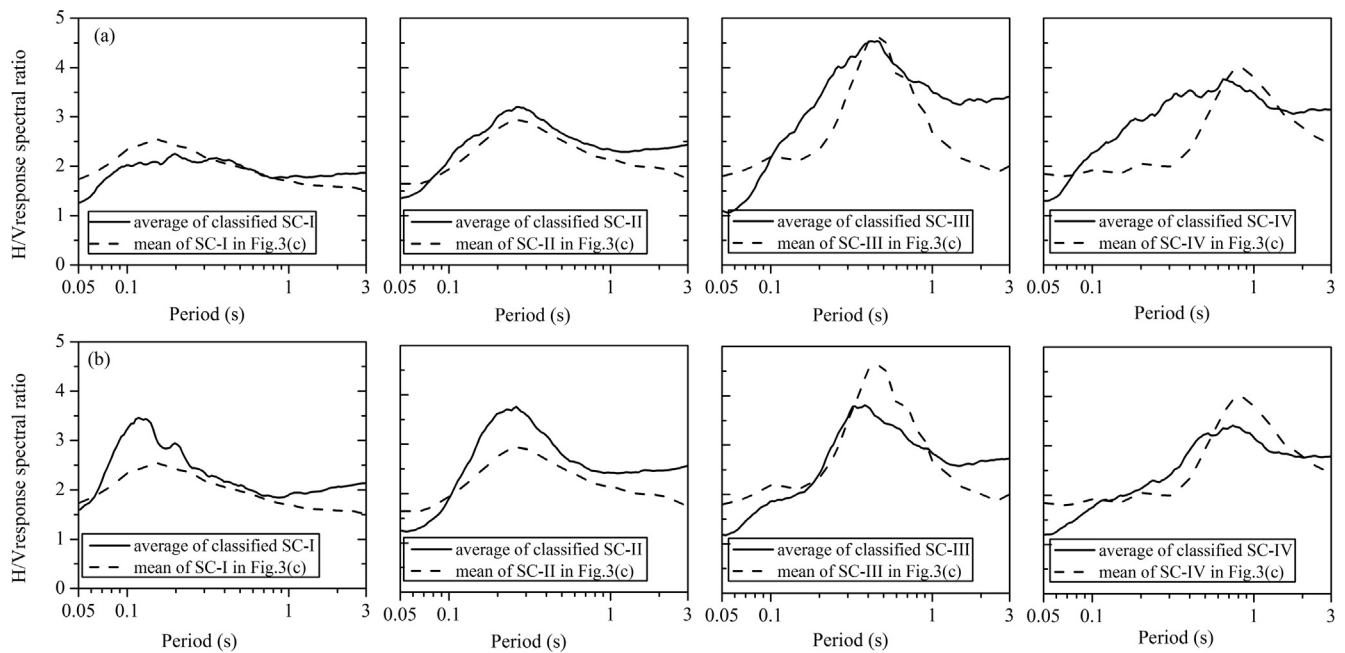


Fig. 14. Comparison between the mean HVSRs of NSMONS recordings (a) using Method 2 and (b) using Method 3 with those proposed by Zhao et al. (2006a) for Japanese strong motion stations.

Table 4
Numbers of NSMONS stations of different site class achieved by different site classification methods.

M1/M2	SC-I	SC-II	SC-III	SC-IV	Total	M1/M3	SC-I	SC-II	SC-III	SC-IV	Total
CL-I	7	7	0	0	14	CL-I	8	2	0	4	14
CL-II	19	64	18	15	116	CL-II	15	70	26	0	111
CL-III	3	15	14	16	48	CL-III	0	0	16	32	48
Total	29	86	32	31	178	Total	23	72	42	36	173

M1: method proposed in this paper.
 M2: method proposed by Zhao et al. (2006a).
 M3: method proposed by Ghasemi et al. (2009).

To improve the classification success rate, an empirical site classification method (Method 1) that comprehensively considers the peak period, amplitude, and shape of the HVSR curve was proposed. To assess its efficiency, 279 stations selected from KiK-net were re-classified using this method and methods proposed by Zhao et al. (2006a) (Method 2) and Ghasemi et al. (2009) (Method 3). It was found that the classification success rates of Method 1 for SC-I, SC-II, and SC-III sites were 63%, 64%, and 58%, respectively, demonstrating overall better performance than either Method 2 and 3.

Using 1281 strong motion recordings obtained from 2007 to 2015, 178 NSMONS stations were classified by our proposed method, among which 14, 116, and 48 stations are CL-I, CL-II, and CL-III sites, respectively. The mean HVSR curve for each site class was re-calculated and compared with standard curve derived using KiK-net data. The comparisons show good consistency in both curve shape and peak period, indicating the efficiency and practicability of the proposed method. Moreover, we collected borehole data from 81 stations and assigned their site classes based on the two indices of V_{S20} and H . Most stations were assigned the same site class as determined using the proposed HVSR method, implying that our site classification results are acceptable.

The site classification method proposed in this study has a relatively high success rate, and it could be considered an optimum alternative method for NSMONS stations before borehole drilling is investigated. Site classification for many more NSMONS stations could be achieved should

additional recordings be accumulated in the future. It should be noted that the HVSR of a given site might contain local topography effects that are inconsistent with the seismic code site class, which is usually based on the shear wave velocity profile of surface soil and bedrock depth. Therefore, further examination of the site classes derived in the present study should be undertaken using surface settings that are more specific, additional geotechnical data, and field investigations.

Acknowledgements

This work was supported by the Scientific Research Fund of the Institute of Engineering Mechanics, China Earthquake Administration No. 2016A04, Nonprofit Industry Research Project of CEA under grant No. 201508005, and Chinese National Natural Science Fund grants No. 51308515. The authors acknowledge China Strong Motion Network Center (CSMNC) for providing the Chinese strong-motion data included in this paper which are freely available upon request from CSMNC (www.csmnc.net; last accessed May 2017). The authors would like to acknowledge the National Research Institute for Earth Science and Disaster Prevention (NIED) in Japan for providing the KiK-net data used in this manuscript. The authors are also grateful to two anonymous reviewers for their valuable comments and suggestions which help in improving the manuscript.

Appendix A

See Table A1.

Table A1
The site classification results for stations of NSMONS of China.

Station code	V ₅₂₀ (m/s)	H (m)	Mb	M1	M2	M3	Station code	V ₅₂₀ (m/s)	H (m)	Mb	M1	M2	M3	Station code	V ₅₂₀ (m/s)	H (m)	Mb	M1	M2	M3
012DAT	134	> 80	CL-III*	CL-III	SC-IV	SC-IV	051SWH	186	4.1	CL-II*	CL-II	SC-II	SC-I	064 GYN	335	20	CL-II*	CL-II	SC-I	SC-II
012DZZ	151	> 50	CL-III*	CL-III	SC-IV	SC-IV	051TQL	281	7.8	CL-II*	CL-II	SC-II	SC-I	064 HSN	274	20	CL-II*	CL-II	SC-I	SC-II
012FTZ	158	> 80	CL-III	CL-III	SC-III	SC-III	051WGW	295	15.88	CL-II*	CL-II	SC-IV	Fail	064 JSN	190	> 30	CL-II*	CL-II	SC-IV	SC-III
012GUG	138	> 80	CL-III*	CL-III	SC-II	SC-II	051YAD	190	18.5	CL-II*	CL-II	SC-II	SC-II	064 NLG	284	> 30	CL-II*	CL-II	SC-II	Fail
012XAZ	154	> 50	CL-III*	CL-III	SC-III	SC-III	051YAL	226	8.3	CL-II*	CL-II	SC-I	SC-I	064 PJB	193	> 30	CL-II*	CL-II	SC-I	SC-III
012ZHB	159	> 50	CL-III*	CL-III	SC-III	SC-III	051YBH	226	8.3	CL-II*	CL-II	SC-I	SC-I	064WUZ	204	26	CL-II*	CL-II	SC-I	SC-III
013DXZ	144	30	CL-III*	CL-III	SC-III	SC-III	051YYL	200	> 35	CL-II*	CL-II	SC-I	SC-III	064YCH	203	> 30	CL-II*	CL-II	SC-III	SC-III
013JZG	183	> 50	CL-III*	CL-III	SC-IV	SC-IV	053BBJ	200	> 35	CL-II*	CL-II	SC-II	SC-II	064YFU	190	> 30	CL-II*	CL-II	SC-IV	SC-II
0140XU	354	> 46	CL-II*	CL-II	SC-IV	SC-IV	053BSL	245	9.6	CL-II*	CL-II	SC-I	SC-I	065AGE	335	20	CL-II*	CL-II	SC-I	SC-II
015BYM	231	> 50	CL-III*	CL-III	SC-II	SC-II	053BNX	327	8.7	CL-II*	CL-II	SC-II	SC-III	065AKT	274	20	CL-II*	CL-II	SC-III	SC-IV
015DKT	231	> 50	CL-III*	CL-III	SC-III	SC-III	053DFY	400	3	CL-I*	CL-I	SC-I	SC-I	065ALL	284	> 30	CL-II*	CL-II	SC-II	SC-III
015TLT	328	50	CL-III*	CL-III	SC-II	SC-II	053DHD	181	> 30	CL-II*	CL-III	SC-I	SC-I	065ALM	203	> 30	CL-II*	CL-II	SC-III	SC-II
015WLH	328	13	CL-II*	CL-II	SC-II	SC-II	053DHL	181	> 30	CL-II*	CL-III	SC-IV	SC-IV	065ATS	204	26	CL-II*	CL-II	SC-II	SC-II
021NQT	271	20	CL-II*	CL-II	SC-III	SC-III	053DJL	245	9.6	CL-II*	CL-II	SC-I	SC-I	065BAC	203	> 30	CL-II*	CL-II	SC-I	SC-II
037LZH	340	22	CL-II*	CL-II	SC-I	SC-I	053DSL	327	8.7	CL-II*	CL-II	SC-III	SC-III	065BKS	203	> 30	CL-II*	CL-II	SC-III	SC-III
051AXY	Rock	22	CL-II*	CL-II	SC-II	Fail	053DPTD	400	3	CL-I*	CL-I	SC-I	SC-I	065CYZ	190	> 30	CL-II*	CL-II	SC-I	SC-II
051BCQ	235	22	CL-II*	CL-I	SC-II	SC-IV	053DZF	400	3	CL-I*	CL-III	SC-IV	SC-IV	065DAQ	190	> 30	CL-II*	CL-II	SC-IV	SC-II
051BTT	220	7.1	CL-II*	CL-II	SC-II	SC-II	053J CZ	336	25	CL-II*	CL-II	SC-III	SC-III	065EBT	203	> 30	CL-II*	CL-II	SC-III	SC-II
051BXZ	245	9	CL-II*	CL-II	SC-II	SC-I	053JPW	336	25	CL-II*	CL-III	SC-I	SC-I	065EJT	203	> 30	CL-II*	CL-II	SC-I	SC-II
051DJH	245	4.2	CL-I*	CL-I	SC-I	SC-I	053JZX	170	18.6	CL-II*	CL-II	SC-II	SC-II	065FCH	203	> 30	CL-II*	CL-II	SC-II	SC-III
051EMS	277	4.2	CL-I*	CL-I	SC-I	SC-I	053LDS/053LDC	170	18.6	CL-II*	CL-II	SC-I	SC-I	065GDL	203	> 30	CL-II*	CL-II	SC-I	SC-III
051GXT	188	11.3	CL-II*	CL-III	SC-II	SC-IV	053LDT	170	18.6	CL-II*	CL-III	SC-II	SC-II	065GLK	203	> 30	CL-II*	CL-II	SC-II	SC-II
051GVZ	245	10.8	CL-II*	CL-II	SC-II	SC-II	053LDT	170	18.6	CL-II*	CL-III	SC-IV	SC-IV	065HLJ	203	> 30	CL-II*	CL-II	SC-IV	SC-II
051HDQ	218	12	CL-II*	CL-II	SC-II	SC-II	053LDT	170	18.6	CL-II*	CL-III	SC-IV	SC-IV	065HQC	203	> 30	CL-II*	CL-II	SC-IV	SC-II
051HDX	243	11.6	CL-II*	CL-II	SC-II	SC-II	053LFB	301	25	CL-II*	CL-III	SC-I	SC-I	065HZW	203	> 30	CL-II*	CL-III	SC-I	SC-IV
051HSD	324	20	CL-II*	CL-I	SC-I	SC-I	053LJH	230	18	CL-II*	CL-III	SC-IV	SC-IV	065IAS	203	> 30	CL-II*	CL-III	SC-IV	SC-IV
051HSS	386	7.6	CL-II*	CL-II	SC-IV	SC-IV	053LLT	250	> 18	CL-II*	CL-II	SC-I	SC-I	065JAS	203	> 30	CL-II*	CL-III	SC-III	SC-IV
051HYV	198	12	CL-II*	CL-II	SC-IV	SC-IV	053LLX	250	> 18	CL-II*	CL-II	SC-III	SC-III	065JG	203	> 30	CL-II*	CL-II	SC-III	SC-IV
051JGS	355	5.7	CL-II*	CL-II	SC-I	SC-I	053LZH	250	> 18	CL-II*	CL-II	SC-III	SC-III	065KX	203	> 30	CL-II*	CL-III	SC-III	SC-IV
051JYC	237	17.5	CL-II*	CL-II	SC-I	SC-I	053MMM	301	25	CL-II*	CL-II	SC-I	SC-I	065KEC	203	> 30	CL-II*	CL-II	SC-I	SC-I
051JYH	311	14	CL-II*	CL-II	SC-I	SC-I	053MMM	301	25	CL-II*	CL-II	SC-IV	SC-IV	065KEK	203	> 30	CL-II*	CL-II	SC-IV	SC-II
051JYV	271	22	CL-II*	CL-II	SC-II	SC-II	053NBD	230	18	CL-II*	CL-II	SC-I	SC-I	065KUC	203	> 30	CL-II*	CL-II	SC-I	SC-II
051JZG	391	16	CL-II*	CL-II	SC-II	SC-II	053NRT	273	13	CL-II*	CL-II	SC-II	SC-II	065KZR	203	> 30	CL-II*	CL-II	SC-II	SC-II
051JZW	265	20	CL-II*	CL-II	SC-II	SC-II	053PDH	273	13	CL-II*	CL-III	SC-I	SC-I	065LOT	203	> 30	CL-II*	CL-II	SC-I	SC-II
051LDL	281	> 20	CL-II*	CL-II	SC-I	SC-I	053PRX	273	13	CL-II*	CL-III	SC-II	SC-II	065MUS	203	> 30	CL-II*	CL-III	SC-II	SC-III
051LDS	340	20.3	CL-II*	CL-II	SC-IV	SC-IV	053QCT/053QQC	Rock	Rock	CL-II*	CL-III	SC-IV	SC-IV	065SCH	203	> 30	CL-II*	CL-III	SC-IV	SC-III
051LSL	213	6.4	CL-II*	CL-II	SC-IV	SC-IV	053QWZ	Rock	Rock	CL-II*	CL-III	SC-I	SC-I	065SLM	203	> 30	CL-II*	CL-III	SC-I	SC-III
051LXK	261	20	CL-II*	CL-II	SC-I	SC-I	053RHT	269	17.8	CL-II*	CL-II	SC-III	SC-III	065SRT	203	> 30	CL-II*	CL-II	SC-III	SC-II
051LXM	272	22	CL-II*	CL-III	SC-IV	SC-IV	053RHT	269	17.8	CL-II*	CL-III	SC-I	SC-I	065SUF	203	> 30	CL-II*	CL-II	SC-I	SC-III
051LXS	230	12.6	CL-II*	CL-II	SC-I	SC-I	053YBX	269	17.8	CL-II*	CL-III	SC-IV	SC-IV	065TSD	203	> 30	CL-II*	CL-II	SC-IV	SC-III
051LXT	227	11	CL-II*	CL-II	SC-I	SC-I	053YCH	269	17.8	CL-II*	CL-III	SC-I	SC-I	065WLG	203	> 30	CL-II*	CL-II	SC-I	SC-III
051MBQ	259	22.3	CL-II*	CL-II	SC-I	SC-I	053YJG	269	17.8	CL-II*	CL-III	SC-II	SC-II	065WPR	203	> 30	CL-II*	CL-III	SC-II	SC-III
051MCL	277	22.3	CL-II*	CL-II	SC-II	SC-II	053YML	269	17.8	CL-II*	CL-III	SC-III	SC-III	065WQT	203	> 30	CL-II*	CL-II	SC-III	SC-II
051MLN	259	22.3	CL-II*	CL-II	SC-II	SC-II	053YPC	269	17.8	CL-II*	CL-III	SC-I	SC-I	065WSL	203	> 30	CL-II*	CL-II	SC-I	SC-II
051MXB	277	22.3	CL-II*	CL-II	SC-II	SC-II	053YRHR	269	17.8	CL-II*	CL-III	SC-II	SC-II	065WZD	203	> 30	CL-II*	CL-III	SC-II	SC-IV
051MXD	300	22	CL-II*	CL-I	SC-II	SC-II	053YX	223	14	CL-II*	CL-II	SC-IV	SC-IV	065XHE	203	> 30	CL-II*	CL-III	SC-IV	SC-III
051MXF	241	> 20	CL-II*	CL-I	SC-II	SC-II	053ZJA	241	20	CL-II*	CL-II	SC-I	SC-I	065XKR	203	> 30	CL-II*	CL-II	SC-I	SC-III
051NNH	318	> 20	CL-II*	CL-II	SC-IV	SC-IV	062MXT	226	14	CL-II*	CL-II	SC-II	SC-II	065YAH	203	> 30	CL-II*	CL-II	SC-II	SC-III
051PID	318	> 20	CL-II*	CL-II	SC-III	SC-III	062TCH	226	14	CL-II*	CL-II	SC-I	SC-I	065YJT	203	> 30	CL-II*	CL-III	SC-I	SC-IV
							062ZM3	168	10	CL-II*	CL-II	SC-II	SC-II	065YMY	203	> 30	CL-II*	CL-III	SC-II	SC-III
							062ZNI	168	10	CL-II*	CL-II	SC-I	SC-I	065YPH	203	> 30	CL-II*	CL-III	SC-I	SC-IV

(continued on next page)

Table A1 (continued)

Station code	V _{s20} (m/s)	H (m)	Mb	M1	M2	M3	Station code	V _{s20} (m/s)	H (m)	Mb	M1	M2	M3	Station code	V _{s20} (m/s)	H (m)	Mb	M1	M2	M3	
051PWN	227	30	CL-II*	CL-I	SC-I	SC-I	063CEH				CL-I	SC-I	SC-I	065YTK				CL-III	SC-II	SC-II	SC-IV
051PWN	394	22	CL-II*	CL-II	SC-II	SC-II	063DCD	239	30	CL-II*	CL-II	SC-II	SC-II	065YXA				CL-II	SC-II	SC-II	SC-II
051PWP	306	15	CL-II*	CL-II	SC-II	SC-II	064BFN	180	> 30	CL-II*	CL-III	SC-III	SC-III	065YYG				CL-II	SC-II	SC-II	SC-IV
051PZT							064CHX	223	> 30	CL-II*	CL-II	SC-I	SC-I	065ZYC				CL-III	SC-IV	SC-IV	SC-IV
051QCS							064FDG	180	> 30	CL-II*	CL-III	SC-II	SC-III								
051SFB	232	1.2	CL-II*	CL-II	SC-IV	SC-II	064GJZ	189	> 30	CL-II*	CL-III	SC-II	SC-IV								

Note: "Rock", means that the site is classified as "rock" according to the geology survey report.

"Fail", the classification result is unacceptable by checking by t-distribution hypothesis.

"/", means that the station code changed.

"Mb", means the site class is assigned by borehole information or geology survey report for some rock sites.

"M1": method 1 proposed in this paper; "M2": method 2 proposed by Zhao et al. (2006a); "M3": method 3 proposed by Ghasemi et al. (2009).

References

Alessandro, C.D., Bonilla, L.F., Boore, D.M., Rovelli, A., Scotti, O., 2012. Predominant-period site classification for response spectra prediction equations in Italy. *Bull. Seismol. Soc. Am.* 102, 680–695.

Allen, T.I., Wald, D.J., 2009. On the use of high-resolution topographic data as a proxy for seismic site conditions (VS30). *Bull. Seismol. Soc. Am.* 99, 935–943.

Bonilla, L.F., Steidl, J.H., Lindley, G.T., Tumarkin, A.G., Archuleta, R.J., 1997. Site amplification in the San Fernando Valley, California: variability of site-effect estimation using the S-wave, Coda, and H/V Method. *Bull. Seismol. Soc. Am.* 87, 710–730.

Boore, D.M., 2004. Estimating VS30(or NEHRP site classes) from shallow velocity models (depths < 30 m). *Bull. Seismol. Soc. Am.* 94, 591–597.

Building Seismic Safety Council (BSSC), 2003. The 2003 NEHRP recommended provisions for new buildings and other structures, Part I (Provisions) and Part II (Commentary), FEMA 368/369, Washington, D.C.

Dai, J.W., Ji, K., Wen, R.Z., Ren, Y.F., 2015. Ground motion characteristic of the Jinggu M_s 6.6 earthquake in Yunnan. *China Earthq. Eng. J.* 37, 969–975 (in Chinese).

European Committee for Standardization (CEN), 2004. Eurocode 8: Design of structures for earthquake resistance – Part 1: General rules, seismic actions and rules for buildings.

Fukushima, Y., Bonilla, L.F., Scotti, O., Douglas, J., 2007. Site classification using horizontal-to-vertical response spectral ratios and its impact when deriving empirical ground-motion prediction equations. *J. Earthq. Eng.* 11, 712–724.

Ghasemi, H., Zare, M., Fukushima, Y., Sinaeian, F., 2009. Applying empirical methods in site classification, using response spectral ratio (H/V): a case study on Iranian strong motion network (ISMN). *Soil Dyn. Earthq. Eng.* 29, 121–132.

Guo, F., 2010. Research on some issues of site for seismic design. [M.S. Thesis] Huazhong University of Science and Technology, Wuhan (in Chinese).

Japan Road Association (JRA), 1980. Specifications for Highway Bridges Part V, Seismic Design. Maruzen Co., LTD.

Ji, K., Wen, R.Z., Cui, J.W., Ren, Y.F., 2014a. Observation of strong motion and damage investigation for M_s 6.5 Ludian earthquake. *Technol. Earthq. Disaster Prevent.* 9, 325–339 (in Chinese).

Ji, K., Wen, R.Z., Ren, Y.F., 2014b. Analysis of site characteristics based on strong-motion records of Lushan aftershocks. *Earthq. Eng. Eng. Dyn.* 34, 35–42 (in Chinese).

Ji, K., Wen, R.Z., Ren, Y.F., 2014c. Estimation of site nonlinear response in Lushan earthquake. *Earthq. Eng. Eng. Dyn.* 34 (S1), 100–105 (in Chinese).

Kuo, C.H., Wen, K.L., Hsieh, H.H., Lin, C.M., Chang, T.M., Kuo, K.W., 2012. Site classification and Vs30 estimation of free-field TSMIP stations using the logging data of EGD. *Eng. Geol.* 129, 68–75.

Kuo, C.H., Wen, K.L., Lin, C.M., Wen, S., Huang, J.Y., 2015. Investigating near surface S-wave velocity properties using ambient noise in Southwestern Taiwan. *Terrest. Atmos. Ocean. Sci.* 26, 205–211.

Lee, C.T., Cheng, C.T., Liao, C.W., Tsai, Y.B., 2001. Site classification of Taiwan free-field strong-motion stations. *Bull. Seismol. Soc. Am.* 91, 1283–1297.

Lermo, J., Chávez-García, F.J., 1993. Site effect evaluation using spectral ratios with only one station. *Bull. Seismol. Soc. Am.* 83, 1574–1594.

Li, X.J., Zhou, Z.H., Yu, H.Y., Wen, R.Z., Lu, D.W., Huang, M., Zhou, Y.N., Cui, J.W., 2008. Strong motion observations and recordings from the great Wenchuan Earthquake. *Earthq. Eng. Eng. Vib.* 7, 235–246.

Lü, H.S., Zhao, F.X., 2007. Site coefficients suitable to China site category. *Acta Seismol. Sin.* 29, 71–79.

Ministry of Housing and Urban-Rural Construction of the People's Republic of China (MHURC), 2010. Code for Seismic Design for Buildings (GB 50011 2010). China Building Industry Press, Beijing (in Chinese).

Nakamura, Y., 1989. A method for dynamic characteristics estimation of subsurface using microtremor on the ground surface. *Quarterly Reports* 30. Railway Technical Research Institute pp. 25–33.

Ren, Y.F., Wen, R.Z., Zhou, B.F., Huang, X.T., 2013. The characteristics of strong ground motion of Lushan earthquake on April 20, 2013. *Chin. J. Geophys.* 57, 1836–1846.

Seed, H.B., Romo, M.P., Sun, J.I., Jaime, A., Lysmer, J., 1988. The Mexico earthquake of September 19, 1985—relationships between soil conditions and earthquake ground motions. *Earthq. Spectra* 4, 687–729.

Spearman, C., 1904. The proof and measurement of association between two things. *Am. J. Psychol.* 15, 72–101.

Takahashi, T., Kobayashi, S., Fukushima, Y., Zhao, J.X., Nakamura, H., Somerville, P.G., 2000. A spectral attenuation model for Japan using strong motion data base, in The 6th International Conference on Seismic Zonation, Palm Springs Riviera Resort, California, 12–15 November 2000.

Tsai, Y.B., Huang, M.W., 2000. Strong ground motion characteristics of the Chi-Chi, Taiwan earthquake of September 21, 1999. Institute of Geophysics, National Central University.

Wald, D.J., Allen, T.I., 2007. Topographic slope as a proxy for seismic site conditions and amplification. *Bull. Seismol. Soc. Am.* 97, 1379–1395.

Wen, K.L., Chang, T.M., Lin, C.M., Chiang, H.J., 2006. Identification of nonlinear site response using H/V spectral ratio method. *Terrest. Atmos. Ocean. Sci.* 17, 533–546.

Wen, R.Z., Ren, Y.F., Zhou, Z.H., Shi, D.C., 2010. Preliminary site classification of free-field strong motion stations based on Wenchuan earthquake records. *Earthq. Sci.* 23, 101–110.

Wen, R.Z., Ren, Y.F., Shi, D.C., 2011. Improved HVSR site classification method for free-field strong motion stations validated with Wenchuan aftershock recordings. *Earthq. Eng. Eng. Vib.* 10, 325–337.

Wen, R.Z., Ren, Y.F., Zhou, Z.H., Li, X.J., 2014. Temporary strong-motion observation network for Wenchuan aftershocks and site classification. *Eng. Geol.* 180, 130–144.

- Wills, C.J., Petersen, M., Bryant, W.A., Reichle, M., Saucedo, G.J., Tan, S., Taylor, G., Treiman, J., 2000. A site-conditions map for California based on geology and shear-wave velocity. *Bull. Seismol. Soc. Am.* 90, S187–S208.
- Wood, H.O., 1908. Distribution of apparent intensity in San Francisco. *The California Earthquake of April 18*, pp. 220–245.
- Yamazaki, F., Ansary, M.A., 1997. Horizontal-to-Vertical spectrum ratio of earthquake ground motion for site characterization. *Earthq. Eng. Struct. Dyn.* 26, 671–689.
- Zhao, J.X., Irikura, K., Zhang, J., Fukushima, Y., Somerville, P.G., Asano, A., Ohno, Y., Oouchi, T., Takahashi, T., Ogawa, H., 2006a. An empirical site-classification method for strong-motion stations in Japan using H/V response ratio. *Bull. Seismol. Soc. Am.* 96, 914–925.
- Zhao, J.X., Zhang, J., Asano, A., Ohno, Y., Oouchi, T., Takahashi, T., Ogawa, H., Irikura, K., Thio, H.K., Somerville, P.G., Fukushima, Ya., Fukushima, Y., 2006b. Attenuation relations of strong ground motion in Japan using site classification based on predominant period. *Bull. Seismol. Soc. Am.* 96, 898–913.
- Zhao, J.X., Xu, H., 2013. A comparison of VS30 and site period as site-effect parameters in response spectral ground-motion prediction equations. *Bull. Seismol. Soc. Am.* 103, 1–18.